Journal of Engineering Mathematics 20: 345–365 (1986)

Mechanics of the onager

V.G. HART * and M.J.T. LEWIS **

* *Department of Mathematics, University of Queensland, St. Lucia, Queensland 4067, Australia*
** *Department of Adult and Continuing Education, University of Hull, Hull, England*

(Received June 18, 1986)

Summary

A mathematical model is proposed, apparently for the first time, for the onager, a late Roman catapult. The elastic energy of the machine is contained in a cylindrical bundle of twisted elastic cords, and, although each cord satisfies a linear stress-strain law, the geometry of the entire bundle causes a torque to be exerted on the moving arm of the onager which is a nonlinear function of the angular deflection of the arm. This torque is used in the nonlinear differential equations of motion which are integrated numerically. Experimental work is described which assists in determining the torque, and in addition supplies ranges for the projectiles for various masses, sling lengths and finger angles (parts of the release mechanism). Predictions from the mathematics are in reasonable agreement with experiment. A new calibration rule for the onager is proposed, based on the numerical integrations, which complements that known since classical times for the two-armed Greek palintone. Finally an appendix contains a discussion of the effect of a buffer on the motion.

1. Introduction

The Greeks invented and developed catapults which derived their power from the energy stored in twisted elastic fibres, either of animal ligament or of horse-hair. The basic stone-throwing version, the palintone, had two such springs mounted vertically with an arm inserted horizontally through the centre of each. The tips of the arms, which pointed outwards when at rest, were joined by a "bowstring". When the centre of the string, which held a pouch for the missile, was drawn back by windlass, the arm tips were pulled backwards and towards each other, thus further twisting the springs; and on release they swung forwards, straightening the string which propelled the missile just like a bowstring discharging an arrow. A great deal is known about the design, and something about the performance, of the palintone (Marsden [5] and [6], *passim*).

Somewhere between A.D. 100 and 300 the Romans developed instead a one-armed version, latterly known as the onager or wild ass, which remained in use until about A.D. 600. Although sometimes applied in field and naval warfare, it was too cumbrous and massive for easy transport, and it found its major role in sieges, both in attack and defence. The palintone could, if sufficiently large, throw a stone of up to 79 kg; and very probably the onager could too. But the surviving information about it is meagre (Marsden [6], pp. 249–265). All we can be sure of is that a single spring, mounted transversely in a wooden frame, held in its centre a single arm which carried at its tip a sling for the stone. The arm was pulled back by windlass, and on release swung forwards in a vertical arc. The sling, which acted as an extension to the arm, had one end fixed while the other had a

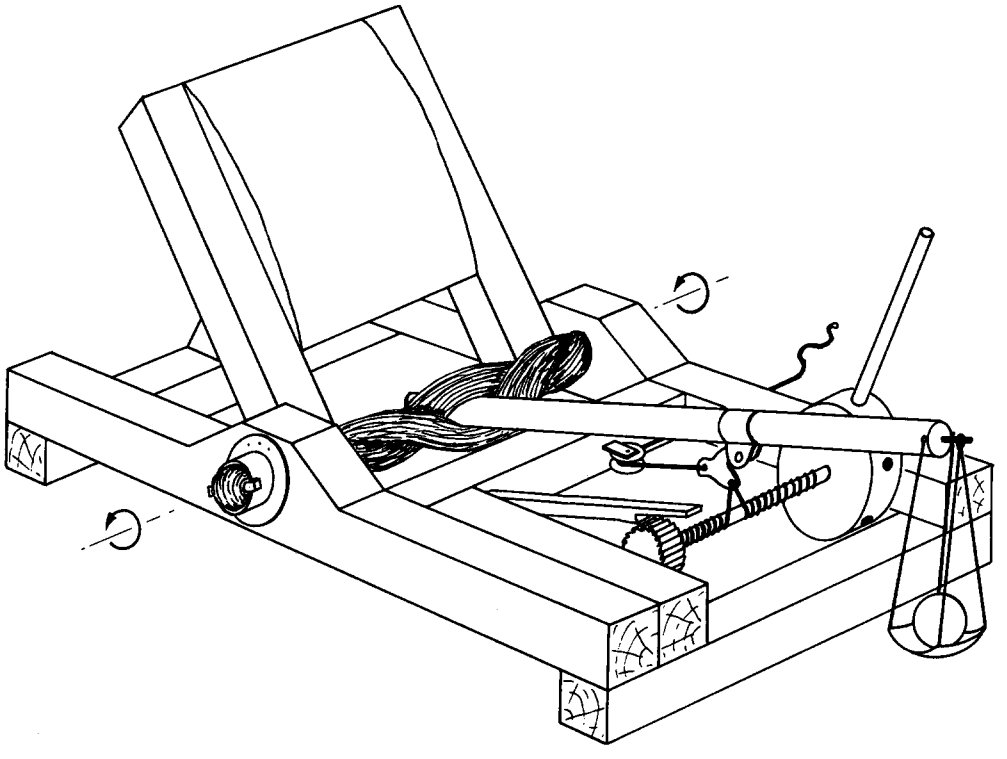

Figure 1. Experimental model onager, drawn with short sling, buffer at 135°, and arm drawn back.

ring that fitted loosely over a pin – the "finger" – projecting from the tip of the arm. At the critical moment during the arm's swing, the ring automatically slipped off the finger, the sling opened and the stone was released. The arm was then arrested by a padded buffer. A reconstruction, necessarily involving much guesswork, appears in Figure 1, and formed the basis for a small machine built for field experiments.

This paper presents, for the first time to the authors' knowledge, a mathematical model for the machine, the resulting predictions being compared with experimental measurements. The nonlinear differential equations of motion are formulated in Section 2, and the torque exerted on the moving arm of the onager by the twisted fibres is calculated in Section 3. Although the individual elastic fibres are supposed to satisfy a linear stress-strain relation the geometry of the entire bundle of fibres implies a nonlinear relation between the torque on the arm and its angular displacement. This torque is derived to agree with experimental results. Section 4 concerns the release mechanism, and the equations are integrated numerically in Section 5 using the torque already mentioned. Results, notably concerning the variation of range with relevant parameters, are contained in Section 6 together with a comparison with observations. The experimental work is described in Section 7.

The design of the two-armed palintone was regulated by a calibration formula (Marsden [6], p. 109) that was evolved about 270 B.C. The Romans no doubt worked out a comparable formula for the onager, but because of the poor survival of later Roman sources it has not come down to us. It is our purpose in Section 8 to use the numerical evidence generated by the mathematical model to propose such a formula.

Although friction and creep of the elastic cords and air resistance are neglected in the model, there is reasonable agreement with experiment – at least as regards variations in range with relevant parameters. An appendix describes the result of inserting a buffer – which in some circumstances may halt the rotation of the arm before the missile is projected. Other recent mathematical work concerning ancient weapons includes Kooi [4] on the bow, and Hart [3] on the palintone. In this paper mathematical work was carried out by the first author while the second author was responsible for the historical account and the experimental work.

2. The equations of motion

The onager, shown schematically in Figure 2, consists of a horizontal spring, cylindrical in form, and with axis O in this figure, made up of a large number of cords of elastic fibre all parallel to the axis of the cylinder except at the ends. Here the cords pass over levers, one at each end of the cylinder and at right angles to the axis, and are securely tied. The levers are each socketed into a metal washer which is embedded in a wooden frame. A uniform rod called an arm (CB in Fig. 2) is inserted through the middle of the fibres at the mid point of the spring cylinder and is held at rest. Both washers are then rotated in the same direction around the virtual axis connecting them as indicated in Figure 1, thus twisting the fibres symmetrically around the arm and exerting a torque on it, and are securely pinned. (It is noted that the cylinders in [3] were incorrectly assumed to be twisted asymmetrically – but the main result of that paper is unaffected by this assumption.) The missile A is placed in a light pouch which is attached to the end B of the arm by four strings of equal length which are supposed to be of negligible mass,

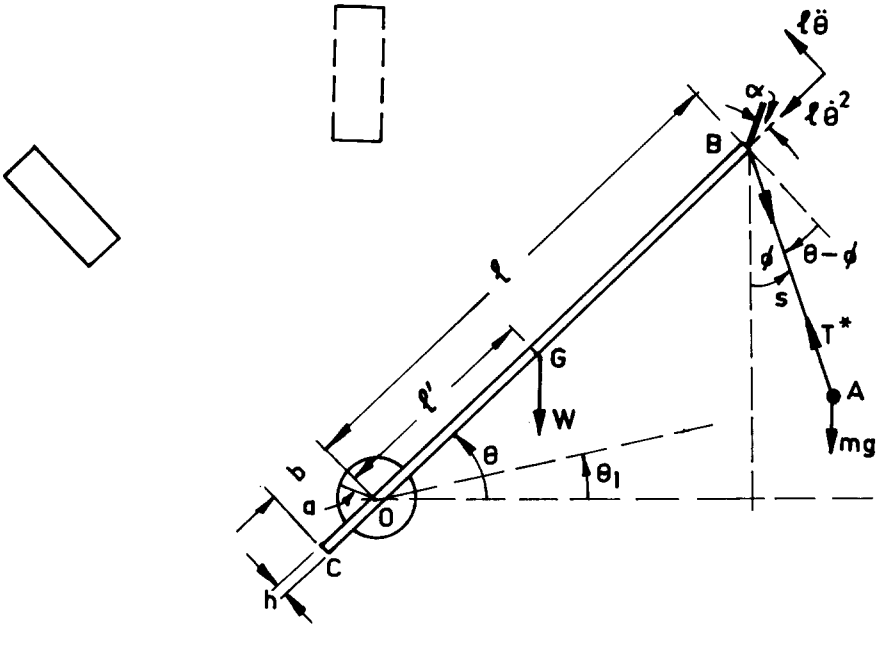

Figure 2. Elevation of the onager, showing two possible positions of the buffer: at $\theta = 90°$ and $\theta = 135°$.

inextensible and perfectly flexible (see Fig. 1). The two lower strings are firmly secured to the arm at B while the two upper strings end in a metal ring which is free to slide over a short rigid metal pin – called a finger – fixed at angle α to the arm. The arm is now wound down to the firing position – at angle θ_1 to the horizontal – by a windlass thus further twisting the fibres of the spring (Fig. 2). On release, the arm is rotated rapidly counterclockwise by the torque in the spring fibres, and the missile in its pouch also rotates around the point B until friction cannot further restrain the ring on the finger. At this point the ring slips off the finger and the missile is launched as in a sling shot. The arm is brought to rest by a buffer shown in Figure 2 either at the vertical position of the arm or at 45° beyond the vertical position. The finger angle α can be varied and its value has a critical effect on the range of the missiles as will be seen.

The equations of motion of the onager are derived as follows. First we note the radial and transverse components of acceleration of B, $l\dot{\theta}^2$ and $l\ddot{\theta}$ as shown in Figure 2. Referring to this figure the second law of Newton for the projectile A, of mass m, resolved along the sling mean direction AB is then

$$ms\dot{\phi}^2 = T^* - mg\cos\phi - ml\left[\ddot{\theta}\cos(\theta-\phi) - \dot{\theta}^2\sin(\theta-\phi)\right], \tag{1}$$

where θ is the angle of inclination of the arm BC with the horizontal, ϕ is the angle between the sling (supposed straight) and the downward vertical through the end B of the arm, s is the sling length, l is the length OB from the axis of rotation of the arm to the end B, g is the acceleration due to gravity and superposed dots indicate time derivatives. Also T^* is the resultant tension in the direction AB.

Also resolving the second law along the perpendicular to BA in the sense of increasing ϕ we get

$$ms\ddot{\phi} = -mg\sin\phi + ml\left[\ddot{\theta}\sin(\theta-\phi) + \dot{\theta}^2\cos(\theta-\phi)\right]. \tag{2}$$

A third basic equation follows from the principle of angular momentum written for the arm about the fixed axis O:

$$I\ddot{\theta} = M - Wl'\cos\theta - T^*l\cos(\theta-\phi), \tag{3}$$

where I is the moment of inertia of arm and spring about the axis O, W is the weight of the arm, $l' = \mathrm{OG}$ and M is the restoring torque exerted on the arm by the spring.

On eliminating T^* between equations (1) and (3) and collecting the terms in $\ddot{\theta}$ we find

$$\ddot{\theta} = \frac{M - Wl'\cos\theta - ml\cos(\theta-\phi)\{s\dot{\phi}^2 + g\cos\phi - l\dot{\theta}^2\sin(\theta-\phi)\}}{I + ml^2\cos^2(\theta-\phi)}. \tag{4}$$

After specification of the torque M and suitable scaling of variables, the nonlinear differential equations (2) and (4) are to be integrated to find the motion. But first we must determine the torque M.

3. The torque exerted by the spring

We consider the spring cylinder of length L and radius a (measured at the inner edge of the cylindrical washers) when untwisted. The upper and lower ends of the fibres are fixed

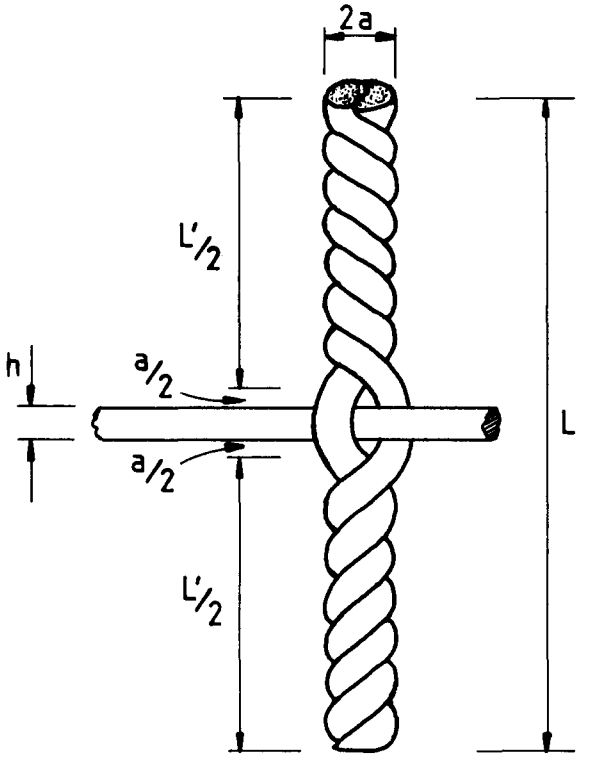

Figure 3. Tightly twisted fibres and torque on the arm.

securely at rest in the washers and the fibres are divided into two half cylinders by the insertion of the arm at mid section. When the fibres are twisted they appear as in Figure 3. It is apparent that the insertion of the arm, of thickness h, causes a distention in the centre of the fibre bundle while the remainder, of total length L' say, can be regarded as of uniform radius. The model proposed for the calculation of the torque on the arm now consists in assuming that both the total length L of the whole bundle and the radius a of the twisted uniform parts are unchanged from the untwisted state, that the distended central part carrying the arm moves as a rigid body rigidly connected to the fibres above and below it, and that the individual fibres are twisted into helices.

We can then easily calculate the torque exerted on the upper cross-section of the central rigid part by finding the traction in the fibres of the uniform upper half cylinder of length $L'/2$. By symmetry the uniform lower half cylinder exerts an equal torque. We therefore now consider the upper half cylinder of length $L'/2$ in Figure 4a in which there are many untwisted elastic fibres all parallel to the axis MN, a typical fibre being marked RS (and S_1T in the lower half cylinder) at a distance r ($\leqslant a$) from the axis. If the arm CB is now twisted through an angle χ to position C'B' (Fig. 4b) the upper half fibre RS is supposed to be stretched into a helix R'S' of pitch angle γ on a cylinder of radius r. The lower half fibre TS_1 is stretched symmetrically to a similar helix $T'S_1'$. The same result is of course obtained if the arm is held fixed and the end washers are rotated in the same direction. Note that the axial fibre MN alone undergoes no stretching with the maximum stretch occurring in the outermost fibres. Although we assume that individual fibres follow a linear stress-strain law of extension, this differential stretching of fibres leads, as

will be seen, to a nonlinear relation between the resultant torque on the arm and its angle χ of rotation relative to the washers. The calculations are as follows.

Taking Cartesian axes *xyz* as shown in Figure 4b, the coordinates of a typical point on a helically deformed fibre in the upper half cylinder are

$$x = r\cos\Phi, \quad y = r\sin\Phi, \quad z = r\Phi\tan\gamma, \tag{5}$$

where Φ is the angle of rotation relative to that point. The arc length of the entire stretched half fibre, initially of length $L'/2$, can be calculated as $L^*/2 = r\chi\sec\gamma$, and the stretch is

$$L^*/L' = (2r\chi/L')\sec\gamma \equiv \Lambda, \tag{6}$$

say. From $(5)_3$ with $\Phi = \chi$ we find

$$L'/2 = r\chi\tan\gamma. \tag{7}$$

Eliminating γ between equations (6) and (7) we find the stretch of a fibre:

$$\Lambda = \left(1 + (2\chi r/L')^2\right)^{1/2}. \tag{8}$$

Next we calculate the torque M exerted by all fibres on the arm. Assuming a continuous distribution of fibres, we integrate the turning action of the upper fibres on the upper part of the central rigid section of the spring cylinder as follows. If τ is the typical fibre stress we have by symmetry for the total torque M:

$$M/2 = 2\pi\int_0^a r^2\tau\cos\gamma\,\mathrm{d}r.$$

Assuming Hooke's law for a fibre,

$$\tau = k(\Lambda - 1), \tag{9}$$

where k is constant, we use equations (6) and (9) to obtain

$$M/2 = 4\pi k(\chi/L')\int_0^a r^3(1 - \Lambda^{-1})\,\mathrm{d}r. \tag{10}$$

Since Λ is given by (8) we find, on performing the necessary integration, that the total torque is given by

$$M/(\pi k a^3) = pa\left[1 - (4/3)(pa)^{-4}\left\{\left(1 + (pa)^2\right)^{3/2} - 3\left(1 + (pa)^2\right)^{1/2} + 2\right\}\right]. \tag{11}$$

Here $p = 2\chi/L'$, and, by observation, we have (see Fig. 3):

$$L' = L - h - a. \tag{12}$$

It must be emphasized that we have neglected friction in and between fibres in calculating the above formula (11).

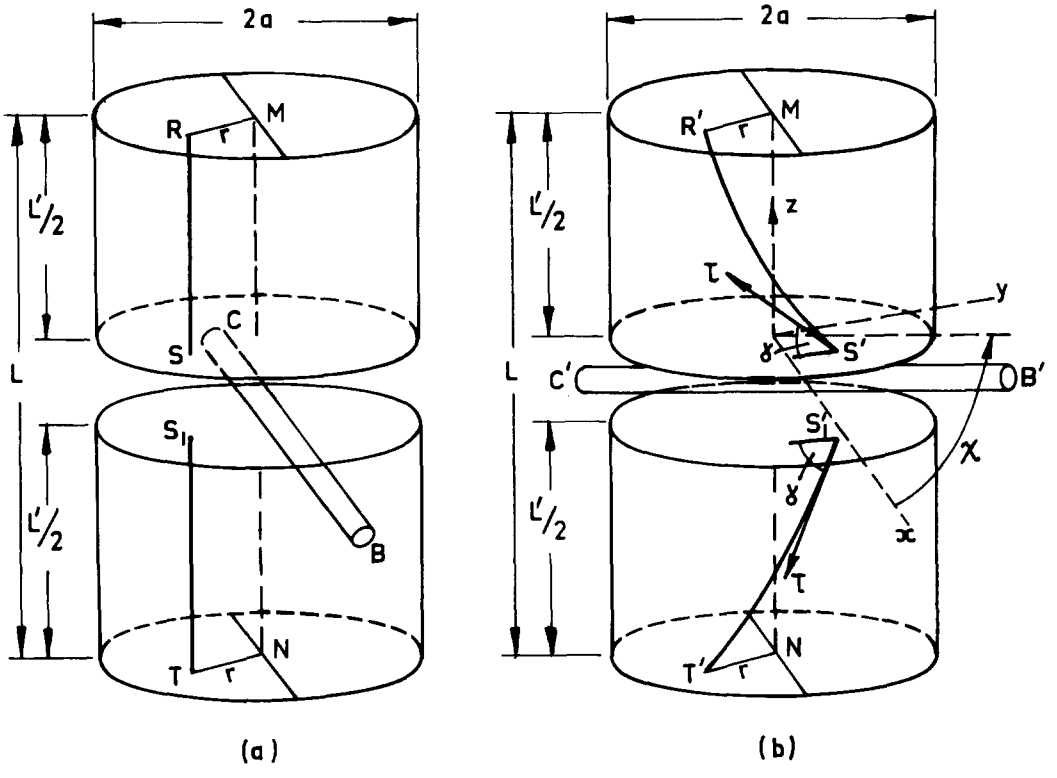

Figure 4. Illustrating twisting of a typical elastic fibre when the arm is rotated through angle χ. The axial fibre MN alone is unextended. (Not to scale).

On comparing the torque/angle relation given by (11) with an experimental investigation of the response of the arm of a typical onager to applied torque, it was found that formula (11) gave a reasonably close prediction of the torque over the experimental range $50° \leqslant \chi \leqslant 170°$. The relation between θ (see Fig. 2) and χ in the specific case considered where $\theta_1 = 15°$ is given by

$$\chi = \tfrac{185}{180}\pi - \theta, \tag{13}$$

radians, and on inserting this value in the expression for p we obtain from (11) the relevant torque as a function of θ for motion of the arm.

To summarise, we write for the torque

$$M = M_0 Q(\theta), \quad M_0 = \pi k a^3, \tag{14}$$

where $Q(\theta)$ is non-dimensional and is given by the right side of equation (11) with

$$pa = \frac{2a}{L'}\left(\tfrac{185}{180}\pi - \theta\right). \tag{15}$$

Here θ is measured in radians. We choose k so that the maximum torque given by (14) agrees with the maximum torque observed in static experiments with the specific machine

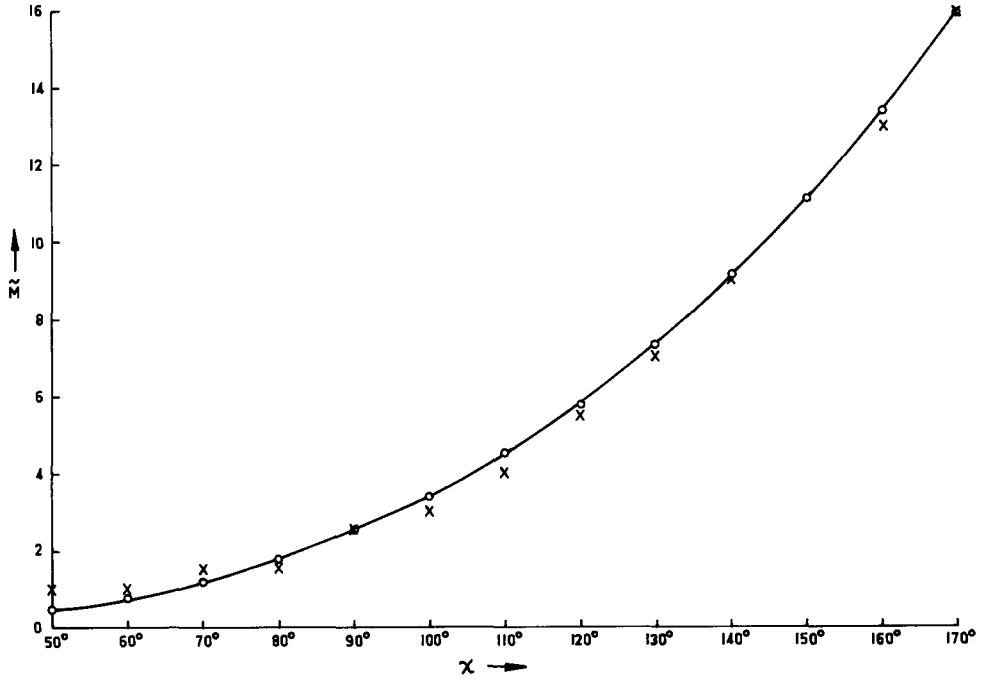

Figure 5. Graph of the nonlinear function (14) (torque against rotation χ of arm) (solid curve) and comparison with experimental points, marked X. $\tilde{M} = 953.53 M/M_0$.

studied. The relation (14) is nonlinear and is shown in Figure 5 together with experimental points.

It is not difficult to derive instead of (11) a form for the torque M based on a finite number of fibres rather than a continuous distribution. However no better fit with experiment is thereby attained, and in this case the continuous distribution leading to (11) is preferable since the integration of the equation (4) is simpler.

It should be remarked that the assumption (9) of Hooke's linear law for the individual fibres appears to be valid for the actual case considered since the maximum strain in outside fibres as calculated by (8) is about 7%, and by experiment the horse-hair fibres used satisfied the linear law (9) up to about 12% strain.

Regarding formula (11) it is also worthy of note that for large pa ($\gg 1$) (large angle of twist χ) the formula reduces to a well-known result. We have $M/M_0 \sim pa$, or

$$M \sim 2\pi k a^4 \chi / L'.$$

This is recognized as the torque for the finite twist of a solid elastic cylinder, and was used in a different application to catapults in Hart [3] – with L' replaced by L. For small pa ($\ll 1$) (small angle χ or long thin cylinder) M/M_0 is approximated by $(pa)^3/3$.

4. The release mechanism

As already mentioned in Section 2 the projectile is carried in a light pouch which is suspended by four light cords from the tip B of the arm – see Figure 1. The two lower

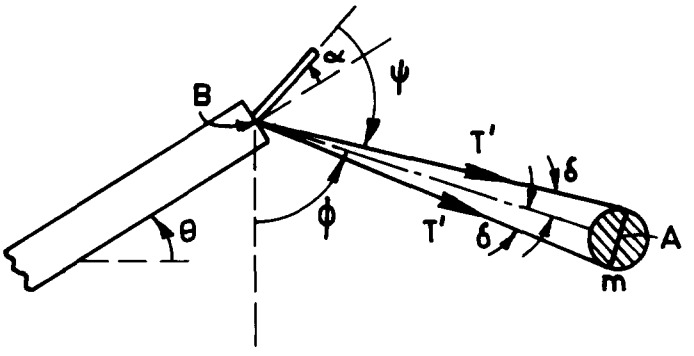

Figure 6. Illustrating the release of the upper cords of the sling on the finger.

cords as shown are fixed to the arm; the two upper cords end at the arm in a metal ring which fits loosely over a "finger" – a thin pin of metal fixed at the arm tip but capable of being set at various finger angles α – measured positively above the centre line of the arm. For simplicity of treatment we replace the forces in the two fixed cords by a single resultant force T', and the forces in the two cords attached to the ring are replaced by a force T' of equal magnitude, these forces being in the vertical plane of symmetry of the arm and equally inclined at angle δ to the line BA – see Figure 6. In terms of the tension T^* used in previous sections we have

$$T^* = 2T' \cos \delta.$$

When the arm is released under tension of the spring, the sling rotates around the moving arm tip B until the angle between the finger and the upper force T' is sufficiently small and friction between the finger and the cord ring can no longer hold the latter at relative rest. When this point is reached the upper cords fly off the finger and the missile is released.

If ψ denote the angle between upper force and finger we have, for no relative motion between the ring and finger (and neglecting the small mass of the ring),

$$F = T' \cos \psi \leqslant \mu P = \mu T' \sin \psi, \tag{16}$$

where F is the force of friction on the ring tangential to the finger, P is the normal reaction, and μ is the coefficient of friction.

From the diagram we note that

$$\psi = \pi - \left(\frac{\pi}{2} - \theta\right) - \phi - \delta + \alpha = \frac{\pi}{2} + \theta - \phi - \delta + \alpha, \tag{17}$$

and equation (16) implies

$$\tan\left(\frac{\pi}{2} + \theta - \phi - \delta + \alpha\right) \geqslant \tan\left(\frac{\pi}{2} - f\right), \tag{18}$$

where f is the angle of static friction: $\tan f = \mu$. The only relevant consequence of (18) is that

$$\theta - \phi \geqslant \delta - f - \alpha, \tag{19}$$

for no slipping of the ring on the finger, and the missile is released when equality holds:

$$\theta - \phi = \delta - f - \alpha. \tag{20}$$

5. Integration of the equations of motion

We now substitute the form (14) derived for the torque exerted by the spring on the arm into equation (4) and integrate numerically the resulting nonlinear differential equation together with (2). First however it is desirable to introduce a dimensionless time variable T and dimensionless parameters η, ϵ, λ, ζ as follows. We set

$$\begin{aligned} &N^2 = M_0/(Ic), \quad T = Nt, \quad \eta = Wl'/(IN^2), \\ &\epsilon = ml^2/I, \quad \lambda = l/s, \quad \zeta = g/(sN^2) = \lambda g/(lN^2). \end{aligned} \tag{21}$$

Here t is the time variable and c is a dimensionless number chosen to ensure a suitably small range of integration in T. Evidently N has dimensions (time)$^{-1}$.

Denoting by dashes derivatives with respect to T equations (4) and (2) become, respectively, on using (14) and (21):

$$\begin{aligned} \theta'' &= \frac{cF(\theta) - \eta \cos\theta - \epsilon\lambda^{-1}\cos(\theta-\phi)\{(\phi')^2 + \zeta\cos\phi - \lambda(\theta')^2\sin(\theta-\phi)\}}{1 + \epsilon\cos^2(\theta-\phi)} \\ &\equiv H, \end{aligned} \tag{22}$$

say, and

$$\phi'' = -\zeta\sin\phi + \lambda\left[H\sin(\theta-\phi) + (\theta')^2\cos(\theta-\phi)\right]. \tag{23}$$

Initial conditions chosen are

$$\theta = \theta_1, \quad \phi = 0, \quad \theta' = \phi' = 0. \tag{24}$$

Equations (22) and (23) were reduced to a set of four first-order equations and were integrated by means of a fourth-order Runge-Kutta method on the University of Queensland DEC-KL10 computer. The subroutine used was the IMSL DVERK [2] and a variety of parameters was considered – but always keeping the initial $\theta_1 = 15°$. The solutions appear to be weakly dependent on the parameters η and ζ and most attention was paid to varying the projectile mass (ϵ) and the sling length (λ).

6. Range, discussion of numerical results and comparison with observation

From the results of numerical integration the general inference for a typical set of parameters is that both θ and ϕ increase monotonically from the initial conditions (24) with $\dot{\theta}$ less than $\dot{\phi}$. This behaviour holds from $T = 0$ up to the point of projection of the missile – which for given α, δ and f is given by equation (20).

If we neglect air resistance the range of the projectile can easily be calculated from elementary theory. Letting the subscript zero refer to the moment of projection, the horizontal and vertical component velocities of the projectile are at this moment:

$$\begin{aligned} v_x &= l\dot{\theta}_0 \sin\theta_0 - s\dot{\phi}_0 \cos\phi_0 = sN(\lambda\theta_0' \sin\theta_0 - \phi_0' \cos\phi_0), \\ v_y &= l\dot{\theta}_0 \cos\theta_0 + s\dot{\phi}_0 \sin\phi_0 = sN(\lambda\theta_0' \cos\theta_0 + \phi_0' \sin\phi_0), \end{aligned} \tag{25}$$

while the angle of projection is

$$\beta = \arctan(v_y/v_x). \tag{26}$$

Then the range of the projectile is $R = 2g^{-1}v_x v_y$, and we define the dimensionless range

$$\hat{R} = gR/(2l^2N^2) = v_x v_y(\lambda sN)^{-2}. \tag{27}$$

Here we have also neglected the height of projection since it is a smaller source of error than neglect of friction. (It would increase maximum ranges by less than 0.2 percent and smaller relevant ranges by less than 2 percent in the cases considered.)

The specific onager studied had the following characteristics. It had a uniform brass arm in the form of a cylindrical tube of mass 51.75 grams, length 193 mm, and diameter 9 mm, which remained almost rigid in the motion. The spring cylinder of horse-hair fibres was of mass 28.35 grams, length $L = 186.4$ mm and radius $a = 10.7$ mm. Thus by (12), $L' = 166.7$ mm. Also, in Figure 2, $l = 175$ mm, $l' = 78.5$ mm. From this information the moment of inertia of the arm about O was calculated at 0.479795×10^{-3} kg m^2, and that of the spring was 0.541×10^{-6} kg m^2. In the latter case the formula mass $\times a^2/6$ was used – corresponding to a continuous cylinder fixed at the ends but with a cross section rotated through an angle proportional to its distance from the nearest end.

The total for I was thus 0.480336×10^{-3} kg m^2. The torque parameter M_0 was chosen as indicated after equation (15) to correspond to the turning action of a weight of 15.949 kg acting at right angles to the arm at a point 98 mm from O with $\theta = 15°$. This implies that $M_0 = 899.3877$ Nm.

Next a trial integration shows that the number c introduced in (21) can be taken as 234.0503 to ensure that the relevant range of integration can be included in the interval $0 \leqslant T \leqslant 2$. This gives $N = 89.4427$ sec^{-1}, and it may be deduced that the typical time of discharge of the onager is about 1/90 seconds. The other parameters in (21) are in this case

$$\eta = 1.037084 \times 10^{-2}, \quad \zeta = 7.007143 \times 10^{-3}\lambda. \tag{28}$$

In calculation, though not in experiment, we consider five sling lengths: $s = 47$, 71, 94, 118 and 141 mm, and in each case three projectile masses (glass marbles): 3.5, 4.9 and 6.3

Table 1. Results for a typical integration of equations (2), (4) (Case 1). The angle of friction on the finger is 50°. Also $\epsilon = 0.2869085$, $\lambda = 3.723404$, $\eta = 1.037084 \times 10^{-2}$, $\zeta = 2.609043 \times 10^{-2}$, $\delta = 2°$.

T	θ_0 degrees	ϕ_0 degrees	α degrees	$\hat{R}$	$u/(sN)$	β degrees
0.60	44	46	−46.6	0.7474	6.5570	75.59
0.80	62	93	−17.4	3.0474	9.4684	54.76
0.91	72	127	7.12	4.1464	11.0143	35.69
0.97	77	148	22.7	3.4786	11.5994	22.90
1.05	84	176	44.2	0.8264	11.8627	4.69

grams. Allowing 1 gram for the pouch and strings this gives

$$\lambda = 3.723404,\ 2.464789,\ 1.861702,\ 1.483051,\ 1.241135,$$
$$\epsilon = 0.2869085,\ 0.3761690,\ 0.4654295, \tag{29}$$

so that in all 15 cases were considered – numbered 1 to 15. Having fixed ϵ and λ, η and ζ are given by (28).

It was convenient in each integration run to print out θ, ϕ, $\dot{\theta}$ and $\dot{\phi}$ for $T = 0$ (0.01) 2.00. Then, for an arbitrary T in this range and with friction angle $f = 50°$, $\delta = 2°$ (by experiment), substitution in (20) of the corresponding values of θ and ϕ gives the finger angle α for release of the projectile at that T. We can also calculate the velocity u at projection, β and $\hat{R}$ from equations (25)–(27). Some typical results obtained in this way are shown in Tables 1 and 2, and in Figure 7.

We note some general trends. From Table 1 for example (for Case 1 and the shortest sling) for increasing finger angle α the missile velocity u at projection increases, but the angle β of projection decreases. The dimensionless range $\hat{R}$ increases to a maximum then decreases, with the maximum in this case being attained at $\alpha = 7.12°$ and projection angle with the horizontal 35.69° (the latter angle varied between 34.2° to 38.2° at maximum $\hat{R}$ in the 15 cases considered). If the missile mass is increased the maximum range $\hat{R}$ is diminished and moves to a larger value of α (e.g. Figure 7a). The effect of lengthening the sling is shown in Figures 7b, 7c. The maximum range increases but there is a decrease of about 22° in the corresponding finger angle for each increase in sling length, with the bell shape of the curves becoming narrower and higher – indicating a greater sensitivity to increasing sling length. A similar decrease in ranges on increasing the missile mass is also noted in Figures 7b, 7c. The smooth solid curves in Figure 7 all correspond to the buffer (Figure 2) being placed at $\theta = 135°$. Some representative data for six cases are presented in Table 2.

The dashed curves in Figures 7b and 7c correspond to results obtained when a buffer is placed at $\theta = 90°$. Such a buffer has no effect on the motion with the shortest sling (Figure 7a) since the missile is launched before the arm reaches the vertical position. But for the two longer slings this situation does not happen and the missile is still in its pouch when the arm strikes the buffer. No rebound occurs due to padding on the buffer and we suppose that the arm comes to rest instantaneously. Details of the resulting motion of the missile are contained in the Appendix but the result on the range $\hat{R}$ curve is to cause a bifurcation from the solid curve at $\theta = 90°$, and it is found that for a finite interval of the finger angle there is a constant range less than the maximum in the unbuffered motion. However, if α is increased sufficiently, a variable but diminishing range again appears.

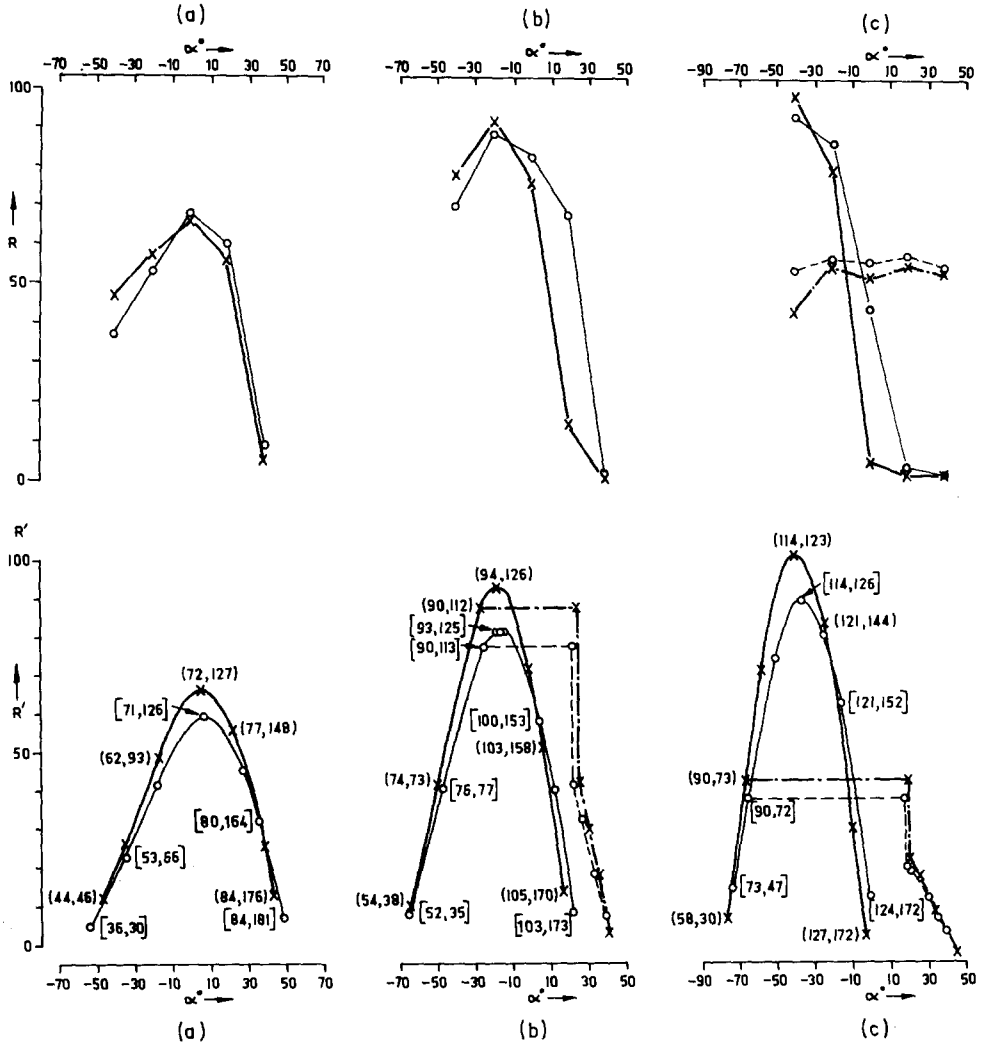

Figure 7 (below). Predicted dimensionless range $R' = 15.929\hat{R}$ against finger angle α (degrees) for three sling lengths s: (a) 47 mm, (b) 94 mm, and (c) 141 mm. Points X refer to projectile mass 3.5 g (Cases 1, 4, 7), points 0 refer to projectile mass 4.9 g (Cases 2, 5, 8). Angles $\theta°$, $\phi°$ are labelled for certain points. Dashed curves correspond to buffer at $\theta = 90°$, solid curves for buffer at $\theta = 135°$ (and at $\theta = 90°$ for Case (a)). Friction angle $f = 50°$, $\delta = 2°$.

Figure 8 (above). Observed range R (metres) against finger angle α (degrees) for three sling lengths s: (a) 47 mm, (b) 94 mm, and (c) 141 mm. Points X refer to projectile mass 3.5 g, points 0 refer to projectile mass 4.9 g. Dashed curves correspond to buffer at $\theta = 90°$, solid curves for buffer at $\theta = 135°$. The solid curves in cases (a) and (b) are also valid for buffer at $\theta = 90°$. Compare with Figure 7. Friction angle $f = 50°$, $\delta = 2°$.

Experimental results appear in Figure 8 and may be compared with the predictions of Figure 7. The scaling has been chosen to make identical the maximum ranges in Figures 7c and 8c referring to the 3.5 g missile. It appears that agreement between the two sets of results is reasonable as regards maximum values of range, finger angles at maxima, increasing range for longer sling with fixed missile mass, and decreasing range with fixed sling length and increasing missile mass – with the maximum shifted to the right. The

Table 2. Prediction and observation compared. Predicted maximum ranges (a) for unresisted motion, (b) with air resistance. Cases 1, 2, 4, 5, 7 and 8. Friction angle $f = 50°$, $\delta = 2°$.

Sling length mm.	Missile mass grams	max. $\hat{R}$	α degrees	(a) max. R metres	(b) max. R metres	R observed, metres
47	3.5	4.1464	7.12	207.1	89	66
	4.9	3.6855	7.30	184.1	86	68
94	3.5	5.7621	−16.7	287.8	104	92
	4.9	5.0626	−16.1	252.9	102	89
141	3.5	6.2778	−38.7	313.6	110	99
	4.9	5.5329	−35.9	276.4	106	94

general shape of the predicted solid curves appears to be verified except that the observations are scanty for cases 8b and 8c to the left of maximum range. Some discrepancy appears however as regards the buffered motion. Observation for the 94 mm sling shows no buffered motion even with the buffer placed at $\theta = 90°$, whereas prediction shows this type of motion for both masses considered (Figures 7b, 8b) and buffer at $\theta = 90°$. Also, although observation for the 141 mm sling now shows the existence of buffered motion, there is a somewhat greater range attached to this motion than is predicted for either of the masses thrown (Figures 7c, 8c).

It is conjectured that these discrepancies may be due to the neglect of friction in and between the elastic fibres in the formulation of the elastic model. Friction would be expected to lead to slower rates of increase in θ and ϕ than those predicted, with the angle $\theta = 90°$ being encountered at greater values of α than those shown in Figure 7c. Also, if the effect of friction were sufficiently great, one could envisage in the case of the 94 mm sling a performance rather similar to that of the 47 mm sling wherein the entire solid curves in Figure 7b are traced out without the angle $\theta = 90°$ being encountered. Evidently the predicted absence of buffered motion for sling length 47 mm and buffer at $\theta = 90°$ is confirmed by observation (Figures 7a, 8a).

All of the previous work assumes that the missile suffers no air resistance. However, an estimate of the range when air resistance is allowed for can be readily made and appropriate comparisons appear in Table 2. These estimates were obtained by use of Figure 6 in the paper of Zufiria and San Martín [9]. Observed ranges vary between 74 and 90 per cent of the theoretical values. Again the comparison appears reasonable considering the neglect of creep and friction between the elastic fibres in the mathematical model.

7. Experimental work

A model onager was built (Figure 1), its design adhering as closely as possible to the meagre information provided by the ancient sources, and adopting what seemed the best features of other modern reconstructions. The main frame was of wood, with steel washers, pull-back mechanism and trigger; a hollow brass arm with a wooden plug to hold the finger; and a thin leather sling attached by fine strings. The spring was made of two-ply horse-hair cord; in default of any information on its proportions, those specified for the palintone were used (1 : 8.7). For the same reason, the length adopted for the arm

was arbitrary, though its approximate length was dictated by the layout of the rest of the machine. Dimensions of spring and arm are given in Section 6. A torque of 1560 kg mm was chosen as being not far short of what the frame would stand; to achieve it the spring was initially twisted from the slack position (fibres parallel) by turning the washers through about 180° before the arm was pulled back, but as the horse-hair stretched in use this pre-tension had gradually to be increased to about 360° in order to maintain the required torque. The arm when drawn back lay at 15° above the horizontal.

The model was tested in a virtually level field on virtually windless days. As described elsewhere, four of the parameters were varied. Three sling lengths were tried, five finger angles, two projectile weights, and two buffer positions. This entailed 60 permutations. For each permutation five shots were fired and their average range was recorded: see Figure 8, and Table 2 for maxima. For reasons of time it was not practicable to vary the other parameters, namely the dimensions of the spring and of the arm.

Because of the relatively small size of the model, absolute precision was impossible. The finger angles could be only approximately measured; the friction between sling ring and finger perhaps varied slightly; the torque was checked (and if necessary adjusted) only every five shots; and it was not possible to mark the point where the projectile hit the ground, only that where it came to rest: it often bounced on impact, usually forwards but sometimes backwards. For all these reasons, the experimental results should not be taken as exact; but they are probably well within 10% of the truth, and they are reasonably consistent.

For practical purposes, the most important results were these.

1. The longer the sling, the greater the maximum range.
2. The longer the sling, the further back (negative α) the finger had to be bent to achieve maximum range.
3. The further back the finger was bent, the higher the trajectory, and the further forward, the flatter. But there is a limit to the backward angle, beyond which the sling slides off the finger when the arm is drawn back; that is why the plots for the medium and long slings on Figure 8 only start at or near the maximum range.
4. With the longest sling, the buffer had to be set at 135° to achieve maximum range, but with the short and medium slings it made no difference whether the buffer was at 90° or 135°.
5. The weight of projectile, within the limits experimented with, made little difference to the maximum range.

The results thus show clearly that a long sling is best. But in practice we may suspect that its very length prevented it from being applied. To allow such a sling to hang free when the arm is drawn back involves raising the whole onager off the ground; easy on a model, difficult with a full-sized version. It could be done; but the extra framework necessary to raise it would markedly increase both the overall weight (with extra problems in transport) and the exposed area of the onager (which would make it more vulnerable to enemy fire). Probably the Romans used nothing longer than the equivalent of our 94 mm sling. Alternatively, as a referee suggests, a longer sling could be fitted if a hole were dug in the ground behind the onager.

This model was by no means the first modern attempt to reconstruct the onager. De Reffye built one about 1860, with buffer inclined forwards and an adjustable finger (Anon. [1]). From 1903 Schramm made two models and a full-sized onager, which incorporated a very short sling and a very short swing for the arm, the buffer being

inclined backwards (Schramm [8] pp. 70–74). At the same time Payne-Gallwey built one with a vertical buffer (Payne-Gallwey [7], pp. 279–299, App. 1 pp. 12–18). And Marsden more recently made a model (Marsden [6], pp. 254–265). Of these, Payne–Gallwey's performed the best, throwing a stone of 3.6 kg – twice what the palintone formula specifies for that size of spring – to over 450 m. Some of these men appreciated the effect of an adjustable finger and of different lengths of sling; but in no case did they carry out any prolonged tests, and they did no experiments – or at least published no results – with altered parameters. Such few figures as are available are of little use because the operating torque was never recorded and the springs were of differing materials. The present trials therefore break fresh ground.

8. A calibration formula for the onager

The Greeks had a rule for the construction of their two-armed palintones or large stone throwing catapults. The first part of it consisted of a calibration formula which gave the diameter of a spring cylinder in terms of the cube root of the mass of the projectile to be thrown:

$$2a = \text{constant}.\ m^{1/3}, \tag{30}$$

[see e.g. Marsen [5], p. 25]. The second part involved a table which gave all other dimensions of the palintone in terms of the spring diameter. No such calibration formula is known for the onager. We propose one here – inferred from the numerical results obtained from the 15 cases of the mathematical model studied. Since the latter gives results comparable with reality it is reasonable to suppose that the calibration formula could be used for the first part of a design programme for onagers, at least over the range of parameters studied in this paper. It should be noted that due to the more complicated model required for the onager it is not possible to give the same type of explicit derivation of the calibration formula that was possible for the palintone in Hart [3].

We propose a least-squares fit of a linear function in the mass and sling length variables ϵ and λ as defined in (21) to the reciprocal of the dimensionless maximum range $\hat{R}_m^{-1}$. Here maximum refers to the greatest value of $\hat{R}$ found in a given case where α varies and all other parameters are fixed (see e.g. Table 1).

Thus we consider

$$1/\hat{R}_m \cong c_0 + c_1\epsilon + c_2\lambda, \tag{31}$$

and find the coefficients c_0, c_1, c_2 by minimising the sum of the squared differences of the right side function in (31) and the predicted values of $\hat{R}_m^{-1}$ given by the mathematical model. We find

$$c_0 = 0.0243042, \quad c_1 = 0.284235, \quad c_2 = 0.0372434, \tag{32}$$

with a root-mean-square error

$$\left(\sum_{i,j} \epsilon_{ij}^2/15\right)^{1/2} = 0.003489,$$

Table 3. Least square fit of $\hat{R}_m^{-1}$ (unbracketed figures) by the linear function in (31) (bracketed figures). Cases 1 to 15 used.

ϵ	λ				
	1.241135	1.483051	1.861702	2.464789	3.723404
0.2869085	0.159291	0.163046	0.173547	0.194336	0.241172
	(0.152078)	(0.161087)	(0.175190)	(0.197651)	(0.244526)
0.3761690	0.180736	0.185554	0.197526	0.220522	0.271333
	(0.177449)	(0.186458)	(0.200561)	(0.223022)	(0.269897)
0.4654295	0.203167	0.209082	0.222624	0.247640	0.302585
	(0.202820)	(0.211829)	(0.225932)	(0.248393)	(0.295268)

ϵ_{ij} being the deviation at a typical point. The pointwise results are shown in Table 3, the figures in brackets being the value given by the right side of (31) and the unbracketed figures the values of $\hat{R}_m^{-1}$ obtained by integration of the equations (2) and (4).

If the result of the above approximation (31) is accepted as being reasonably valid over the intervals of ϵ and λ considered (which we consider reasonably representative of the practical situation) the calibration formula is at once deduced. For we have by (31)

$$\hat{R}_m = gR_m/(2l^2N^2) = \left(c_0 + c_1 ml^2/I + c_2\lambda\right)^{-1}, \tag{33}$$

where R_m is maximum range for varied α with all other parameters fixed. Let us now assume that, as with the palintone, all dimensions in the onager are scaled by the elastic spring radius a. Thus we assume that

$$s = k_1 a, \quad l = k_2 a, \quad I = k_3 a^5, \quad M_0 = k_4 a^3, \tag{34}$$

where k_i are constants independent of a, and (14) was used. Then by (21) and (34) $N^2 = k_4(ck_3)^{-1}a^{-2}$, and, after rearranging, we find from (33) that

$$R_m = (\Lambda^*/g)a^3/\left(m + qa^3\right), \tag{35}$$

with

$$\Lambda^* = 2k_4(cc_1)^{-1}, \quad q = k_3\left(c_1k_2^2\right)^{-1}(c_0 + c_2\lambda).$$

We recognise in (35) the type of dependence of maximum range on spring radius a obtained for the palintone in Hart [3]. Thus R_m tends to an asymptotic limit as a increases, and again there is a point of decreasing advantage for increase of a. This point, if taken as the point of inflexion of the graph of R_m, gives the distinctive value

$$a = a_0 = (m/2q)^{1/3},$$

or, on restoring the original constants,

$$a_0 = \left(c_1k_2^2m/[2k_3(c_0 + c_2\lambda)]\right)^{1/3}. \tag{36}$$

The corresponding maximum range is

$$R_m(a_0) = c_1 k_2^2 \Lambda^* / [3gk_3(c_0 + c_2\lambda)]. \tag{37}$$

Formula (36) is proposed as the calibration formula for the onager. It has a similar cube-root dependence on the mass m to equation (30), but the sling length ratio λ ($= l/s$) now enters the denominator. Evidently by (36) and (37) both the spring radius a_0 at the point of inflexion and the corresponding range increase with lengthening sling.

Although the Greeks and Romans certainly used the calibration formula (30), equation (36) is too complicated for them to have applied, at least in this form. Now, however, a practical application of formula (36) would start by fixing λ at some numerical value – probably corresponding to the longest practical sling. Then the mass m to be thrown would be chosen and a_0 follows from (36), the constants k_2 and k_3 being known or deduced from the palintone specifications. The constants given in (32) are expected to be valid for a considerable range of machine size since their derivation concerns the dimensionless formulation (31). The formula $(34)_2$ then supplies the arm parameter l, and the sling length follows from $s = l/\lambda$. As a check (36) gives $a_0 = 9.17$ mm for $m = 4.9$ g and sling length 141 mm; also $a_0 = 6.20$ mm for $m = 3.5$ g and sling length 47 mm with $l = 175$ mm in both cases. Since in our experimental machine $a = 10.7$ mm it would seem that this machine was somewhat overpowered if (36) is taken as the criterion.

Appendix. Buffered motion

If the arm is stopped in its motion by striking a buffer (Figure 1) before the missile is released the range is in general considerably reduced. Referring to Figure 9 we suppose that the sling makes an angle ϕ_0 with the downward vertical, with the missile at point A, at the instant when the arm strikes a buffer set at $\theta = 90°$. In all practical cases considered we found that $0 < \phi_0 < 180°$ and this condition is assumed in the following. The buffer is padded and no rebound of the arm occurs.

In the above circumstances at impact the sling goes slack and the missile, still in its pouch, is projected on a parabolic path with initial velocity u_0 and at angle β_0 to the horizontal. This motion continues until the point A′ is reached where the sling is again taut. At this point one of two things may happen: either the sling makes a small enough angle with the finger to overcome friction and to enable the ring to slip off the finger instantly and thus launch the missile, or this angle is too large, an impulse is imparted to the projectile and the circular motion is resumed until the angle between sling and finger is small enough to enable the ring to slip off and to launch the projectile. (A third possibility at A′: that the angle between sling and finger is too large for slipping of the ring and continues to increase, involves values of α that are too negative for practical application and is omitted – see after (A6)). The conditions for the first case to occur pertain to a finite interval of values of α, and the range attained by the projectile is the same for all and corresponds to the conditions at A. For larger values of α reduced ranges occur and typical cases are indicated in Figure 7 for the two longer slings. The details are as follows.

Given the condition of a parabolic trajectory issuing from A (Figure 9), the point A′ is found by finding the intersection of this parabola with the circle with centre at the arm

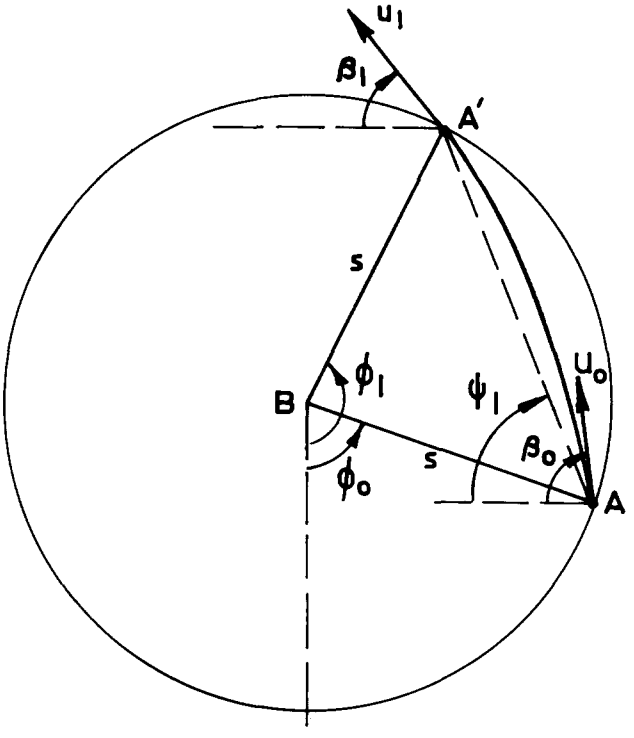

Figure 9. Illustrating projectile motion when arm strikes buffer at $\theta = 90°$.

end B and radius s. This leads to the solution of a cubic equation in D ($= \tan \psi_1$) where ψ_1 is as shown in Figure 9:

$$D^3 - D^2 \tan \beta_0 + (1 + \delta')D + \delta' \tan \phi_0 - \tan \beta_0 = 0, \tag{A1}$$

where

$$\delta' = \zeta(Ns/u_0)^2 \cos \phi_0 \sec^2 \beta_0. \tag{A2}$$

Thus the point A′ is known. (In practice ψ_1 differs little from β_0.) We can now find

$$\phi_1 = 2\pi - 2\psi_1 - \phi_0. \tag{A3}$$

Next the condition for no release of the ring on the finger in position A′ is that friction $F < \mu P$ (as in Sec. 4) or (see Figure 10)

$$T' \cos(\pi - \phi_1 - \delta + \alpha) < \mu T' \sin(\pi - \phi_1 - \delta + \alpha). \tag{A4}$$

This condition leads to $\tan(\pi - \phi_1 - \delta + \alpha) > \mu^{-1}$, or

$$\alpha > \phi_1 - \pi/2 - f + \delta. \tag{A5}$$

Equally there will be immediate release of the missile at A′ if

$$\alpha < \phi_1 - \pi/2 - f + \delta. \tag{A6}$$

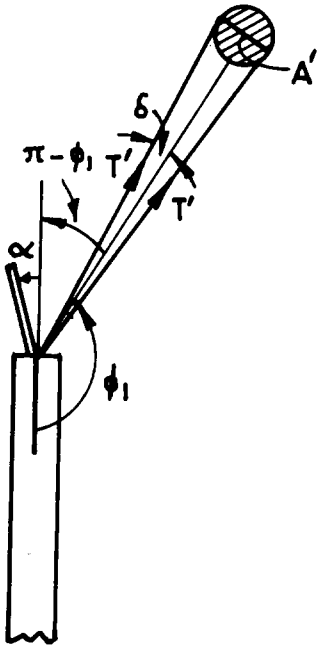

Figure 10. Release condition at the finger illustrated.

In Figure 10 the sling is shown to the right of the finger; a situation of no release of the missile is also reached if the sling direction is far enough to the left of the finger. And this leads to a lower bound on α in (A6) for immediate release – but the values implied are sufficiently negative to be irrelevant to the examples discussed here.

Thus if condition (A6) applies then the missile inherits the range associated with the launch conditions at point A and the horizontal dashed segments in Figures 7b and 7c result.

However for greater values of α, where (A5) applies, the missile undergoes an impulse which brings it back to the circular path around B. The initial tangential speed after this impulse can be calculated as

$$u_1' = -u_1 \cos(\beta_1 + \phi_1), \tag{A7}$$

where u_1, β_1 refer to the particle motion at A′ just before the impulse (Figure 9).

We can calculate these quantities from the parabolic motion of the missile as follows:

$$u_1 = (\dot{x}^2 + \dot{y}^2)^{1/2}, \quad \beta_1 = \arctan(\dot{y}/\dot{x}),$$

where, at A′,

$$\dot{x} = u_0 \cos \beta_0, \quad \dot{y} = u_0 \sin \beta_0 - g x_{A'}/(u_0 \cos \beta_0),$$

and $x_{A'}$, the abscissa of A′ relative to A, is given by geometry as

$$x_{A'} = 2s \sin(\psi_1 + \phi_0) \cos \psi_1.$$

The particle then continues in the circular path until the release condition is encountered at $\phi = \phi_2$ where

$$\phi_2 = \pi/2 + \alpha + f - \delta. \tag{A8}$$

The tangential velocity u_2 at this point is the initial velocity of projection of the missile and is given by the usual energy considerations. We find, on using (A3), (A7) and (A8):

$$u_2^2(Ns)^{-2} = (u_1')^2(Ns)^{-2} - 2\zeta(\cos\phi_1 - \cos\phi_2), \tag{A9}$$

and the dimensionless range, as in (27), is given by

$$\hat{R} = -u_2^2(\lambda Ns)^{-2} \sin\phi_2 \cos\phi_2, \tag{A10}$$

on substitution from (A8) and (A9). The remaining parts of the dashed graphs in Figures 7b and 7c then follow.

Acknowledgements

The first author is grateful to University College, Dublin, for hospitality extended on a recent leave, also to Dr D. Judge of that College and to Mr J. Zornig of the University of Queensland for assistance in computer programming.

References

[1] Anon, Les modèles d'armes romaines du Musée de Saint-Germain, *La Nature* 119 (1875) 231–234.
[2] S.D. Conte and C. de Boor, *Elementary Numerical Methods*, Third Edition. New York: McGraw-Hill Publishers (1980).
[3] V.G. Hart, The law of the Greek catapult, *Bulletin of the Institute of Mathematics and its Applications* 18 (1982) 58–63.
[4] B.W. Kooi, On the mechanics of the bow and arrow, *Journal of Engineering Mathematics* 15 (1981) 119–145.
[5] E.W. Marsden, *Greek and Roman Artillery, Historical Development*. Oxford: Clarendon Press Publishers (1969).
[6] E.W. Marsden, *Greek and Roman Artillery, Technical Treatises*. Oxford: Clarendon Press Publishers (1971).
[7] R. Payne-Gallwey, *The Crossbow*, Second Edition. London: Holland Press (1958).
[8] E. Schramm, *Die antike Geschütze der Saalburg*, reprint. Bad Homburg: Saalburgmuseum (1980).
[9] J.A. Zufiria and J.R. Sanmartín, Influence of air drag on the optimal hand launching of a small round projectile, *American Journal of Physics* 50 (1982) 59–64.